Electron Paramagnetic Resonance Spectroscopy of the Iron−Molybdenum Cofactor of *Clostridium pasteurianum* Nitrogenase

Graham N. George,*,† Roger C. Prince,‡ and Richard E. Bare‡

Stanford Synchrotron Radiation Laboratory, Stanford University, SLAC MS 69, P.O. Box 4349, Stanford, California 94309, and Exxon Research and Engineering Company, Route 22 East, Annandale, New Jersey 08801

Received June 15, 1995[⊗]

We report a computer simulation study of the electron paramagnetic resonance (EPR) spectral line shape of the iron−molybdenum cofactor of nitrogenase. The unusually broad and asymmetric line shape of the EPR spectrum can be interpreted in terms of a distribution of zero-field splitting parameters called *D*-strain. The best fit simulations were computed using $D = 2.5$ cm^{-1} and $E = 0.317$ cm^{-1} and distributions in *D* and *E* approximated by Gaussians of half-widths 0.446 cm^{-1} and 0.108 cm^{-1}, respectively. The value of *D* estimated in the present work is smaller than previous estimates by others but consistent with the temperature dependence of the EPR spectrum. The large *D*-strain is most likely caused by an ensemble of nearly isoenergetic conformational states and should not be considered as being indicative of chemical inhomogeneity.

Introduction

The six-electron reduction of nitrogen (N_2) to ammonia is arguably the most difficult chemical reaction known in biology. While thermodynamically favorable ($\Delta G° = -16.6$ kJ mol^{-1}), the reaction involves breaking the extremely strong N≡N triple bond (941 kJ mol^{-1}) at a reasonable rate. The biological reduction of nitrogen to ammonia, often called nitrogen fixation, is catalyzed by the enzyme complex known as nitrogenase. Many bacteria are capable of nitrogen fixation, and despite considerable taxonomic diversity (*e.g.* ref 1), their nitrogenase systems appear remarkably similar.[2]

There are two protein components of nitrogenase. The smaller iron protein contains a single Fe_4S_4 cluster and supplies electrons in an ATP-dependent process to the larger protein, which, in turn, catalyses the N_2 reduction. In most cases the latter is a molybdenum−iron protein, although vanadium and iron may substitute for molybdenum in alternative nitrogenase systems.[3,4] The molybdenum−iron protein contains two different types of cluster, called P and M clusters. The former type appears to be two Fe_4S_4 clusters in close association[5,6] and the latter a novel iron−sulfur molybdenum cluster[5,6] which also contains homocitrate.[7] The M cluster is thought to be the active site of N_2 reduction and can be extracted from the protein using organic solvents as a low-molecular-weight cofactor called the iron−molybdenum cofactor, or FeMo-co (see ref 8 and references therein). The crystal structures of the molybdenum−iron proteins from *Azotobacter vinelandii*[5] and *Clostridium pasteurianum*[6] have been solved. This work confirms that the M cluster is indeed a Mo−Fe−S cluster, and complete structural models of the active site have been presented (although there remains some controversy over the precise structural details).[5,6] Structural refinements of the crystallographic information have also been attempted using X-ray absorption spectroscopy.[9,10] Despite the wealth of information that is now available on the nitrogenase system, the exact catalytic mechanism, and even the nature and location of N_2 binding to the M cluster, remains unknown, although we note that some interesting hypotheses have been forwarded.[11,12]

In the as-isolated reduced state, both the protein and FeMo-co possess $S = {}^3/_2$ ground states, with positive zero-field splittings, that give rise to well-defined EPR signals from the $\pm{}^1/_2$ Kramers doublet. These signals have been used in numerous investigations of the chemistry and biochemistry of the nitrogenase active site[13−16] (also see ref 8 for additional references). While the protein EPR signal has quite sharp line widths, the FeMo-co signal possesses relatively broad, asymmetric features (*e.g.* ref 8 and references therein).

EPR spectroscopic studies of both Kramers and non-Kramers systems have shown that the zero-field splitting is best described as a statistical distribution of values rather than as a finite value.[17−21] Distributed spin Hamiltonian parameters are well-

* To whom correspondence should be addressed.
† Stanford.
‡ Exxon.
[⊗] Abstract published in *Advance ACS Abstracts,* December 1, 1995.

(1) Woese, C. R. *Microbiol. Rev.* **1987**, *51*, 221−271.
(2) Postgate, J. R. *Fundamentals of Nitrogen Fixation*; Cambridge University Press: Cambridge, U.K., 1982.
(3) Robson, R. L.; Eady, R. R.; Richardson, T. H.; Millar, R. W.; Hawkins, M.; Postgate, J. R. *Nature* (*London*) **1986**, *332*, 388−390.
(4) Chisnell, J. R.; Premakumar, R.; Bishop, P. E. *J. Bacteriol.* **1988**, *170*, 27−33.
(5) (a) Kim, J.; Rees, D. C. *Science* **1992**, *257*, 1677−1681. (b) Chan, M. K.; Kim, J.; Rees, D. C. *Science* **1993**, *260*, 792−794.
(6) (a) Bolin, J. T.; Ronco, A. E.; Morgan, T. V.; Mortenson, L. E.; Xuing, N.-H. *Proc. Natl. Acad. Sci. U.S.A.* **1993**, *90*, 1078−1082. (b) Kim, J.; Woo, D.; Rees, D. C. *Biochemistry* **1993**, *32*, 7104−1082.
(7) Hoover, T. R.; Imperial, J.; Ludden, P. W.; Shah, V. K. *Biochemistry* **1989**, *28*, 2768−2771.
(8) Stiefel, E. I.; George, G. N. In *Bioinorganic Chemistry*; Bertini, I., Gray, H. B., Lippard, S. J., Valentine, J., Eds.; University Science Books: Mill Valley, CA, 1994; pp 365−453.
(9) Liu, H. I.; Filipponi, A.; Gavini, N.; Burgess, B. K.; Hedman, B.; Di Cicco, A.; Natoli, C. R.; Hodgson, K. O. *J. Am. Chem. Soc.* **1994**, *116*, 2418−2423.
(10) Chen, J.; Christiansen, J.; Campobasso, N.; Bolin, J. T.; Tittsworth, R. C.; Hales, B. J.; Rehr, J. J.; Cramer, S. P. *Angew. Chem., Int. Ed. Engl.* **1993**, *32*, 1592−1594.
(11) Deng, H.; Hoffman, R. *Angew. Chem., Int. Ed. Engl.* **1993**, *32*, 1062−1065.
(12) Dance, I. *Aust. J. Chem.* **1994**, *47*, 979−990.
(13) Rawlings, J.; Shah, V. K.; Chisnell, J. R.; Brill, W. J.; Zimmermann, R.; Münck, E.; Orme-Johnson, W. H. *J. Biol. Chem.* **1978**, *253*, 1001−1004.
(14) George, G. N.; Bare, E.; Jin, H.; Steifel, E. I.; Prince, R. C. *Biochem. J.* **1989**, *262*, 349−352.
(15) Venters, R. A.; Nelson, M. J.; McLean, P. A.; Hoffman, B. M.; Orme-Johnson, W. H. *J. Am. Chem. Soc.* **1986**, *108*, 227−236.
(16) True, A. E.; McLean, M. J.; Orme-Johnson, W. H.; Hoffman, B. M. *J. Am. Chem. Soc.* **1990**, *112*, 651−657.

0020-1669/96/1335-0434$12.00/0

known in the form of *g*-strain (*e.g.* ref 22) and have also been detected for the hyperfine interaction (called *A*-strain).[23−24] In the present study we have used computer simulations of the FeMo-co and nitrogenase MoFe protein EPR spectra to show that the line shape anisotropy, and in particular the novel asymmetric line shape of FeMo-co, can be explained in terms of a distribution of zero-field splittings (that can be called *D*-strain).

Materials and Methods

Sample Preparation. *Clostridium pasteurianum* was grown[25,26] in a 400-L fermenter (New Brunswick Scientific Co., Edison, NJ) and the molybdenum−iron protein, isolated by a modification of the procedure of Zumft and Mortenson.[27] The iron−molybdenum cofactor was isolated in *N*-methylformamide solution by a modification of the HCl/NaOH procedure of Yang *et al*.[28]

EPR samples were prepared as frozen *N*-methylformamide FeMo-co solutions containing approximately 1.0 mM molybdenum. EPR spectra were recorded as previously described,[29] with typical instrument settings of 0.5 mT modulation amplitude and 0.1 mW microwave power, unless otherwise stated. Sample temperature was regulated using an Oxford Instruments ESR900 liquid helium cryostat, which had been previously calibrated using a carbon resistor; the error in temperature was found to be within 5% in the temperature range studied. Sample heights were kept small (*ca*. 1 cm) so as to minimize the temperature gradient across the sample.

Computer Simulations. EPR spectra of systems with spin $S > {}^1/_2$ are commonly interpreted in terms of the simple spin Hamiltonian

$$H = \beta_e \mathbf{B}\cdot\mathbf{g}\cdot\mathbf{S} + D[S_z^2 - {}^1/_3 S(S+1)] + E(S_x^2 - S_y^2) \qquad (1)$$

in which all symbols have their usual meanings.[30] β_e is the Bohr magneton, **B** the static magnetic field vector, **S** the electron spin vector, and **g** the *g* tensor; *D* and *E* are the magnitude and the asymmetric zero-field splitting parameters, respectively. *D* and *E* describe the spin energy levels in zero magnetic field and reflect the symmetry of the spin environment. When $D \gg h\nu$ (with $\nu = 9$ GHz, $h\nu \approx 0.3$ cm^{-1}), EPR spectra depend very little on *D*, and it is common practice to explain spectra in terms of a rhombicity $\lambda = E/D$, which is dependent only on the asymmetry of the zero-field splitting. In this case the zero-field splitting Δ is approximately given by $\Delta \approx 2D(1 + 3\lambda^2)^{1/2}$.

Simulations were calculated using Digital Equipment Corp. VAX and Alpha graphics workstations. Two different computer programs were written: an approximate one based upon a perturbation solution and a more exact one based upon diagonalization of the spin Hamiltonian matrix. This latter program differs somewhat from others in the literature [*e.g.* refs 31−33], and we will briefly describe it.

The distribution in zero-field splitting is approximated by assuming Gaussian distributions of *D* and *E*, of respective half-widths σ_D and σ_E, and integrating (by summing individual weighted powder line shapes) over suitable ranges. By analogy with the now-familiar term *g*-strain, we will refer to a distribution in zero-field splittings as *D*-strain. Powder line shapes for individual values of *D* and *E* are calculated by integrating (using Gaussian quadrature) Gaussian spin-packet line shapes, with positions and intensities calculated by matrix diagonalization, over all orientations of magnetic field within an appropriate portion of a sphere. Resonance fields and transition intensities for individual magnetic field orientations are calculated using the following method. The $(2S + 1) \times (2S + 1)$ spin Hamiltonian matrix is constructed for a particular orientation and diagonalized using EISPAK[34,35] routines to obtain the eigenvalues for a grid of equally spaced magnetic fields spanning the range of the spectrum. The resulting curves, which describe the magnetic field dependence of the energy levels, are then interpolated using piecewise cubic splines. Resonances occur when the separation between two energy levels (ΔE) is equal to the microwave quantum, $h\nu$, *i.e.* $\Delta E = h\nu$. A search for $(\Delta E - h\nu) \rightarrow 0$ is then conducted using a Newton−Raphson algorithm for all possible transitions. Any resonance fields found in this way are checked for accuracy by redetermining the eigenvalues at each resonance field. Finally, the eigenvectors are calculated at the resonance fields, and from these the transition probabilities, with the appropriate temperature-dependent Boltzman weighting, are calculated.[32,36−38] The program can generate simulations either for the standard perpendicular mode with the microwave field $\mathbf{B_1} \perp \mathbf{B}$ or for the parallel mode with $\mathbf{B_1} \parallel \mathbf{B}$. Although rather computer-processor intensive, this method yields very accurate simulations.

The perturbation-solution-based program is very much faster and yields a more approximate simulation. Unlike the matrix diagonalization program, this program includes only transitions within the $\pm{}^1/_2$ Kramers doublet and is limited to the $S = {}^3/_2$ case. The greater speed of this program allowed us to use least-squares refinement to obtain approximate values for the spin Hamiltonian parameters. These were then further refined by using the matrix-diagonalization program, manually changing the parameters and judging the quality of the simulation by eye. We estimate that, in general, *g* values can be determined to somewhat better than 1%, *D* to better than 25%, and *E* to within 5%, although we note that manually fitting spectra in the manner described precludes a rigorous determination of uncertainties in the obtained spin Hamiltonian parameters.

Results and Discussion

General Features and Temperature Dependence of the Spectrum. EPR spectroscopy has been used as a tool in numerous investigations of FeMo-co over many years, and the general features of the spectrum are well understood.[8,11] The EPR spectra of FeMo-co in solution in *N*-methylformamide at two different temperatures are shown in Figure 1A. The spectra are typical for a low-symmetry $S = {}^3/_2$ system where $D > h\nu$. The clearly-defined rhombic EPR spectrum, with effective *g* values (*g*′ values) at 4.7, 3.2, and 2.0, derives from transitions within the $\pm{}^1/_2$ Kramers doublet of the $S = {}^3/_2$ system. The true *g* values are almost certainly close to 2.0, and the observed

(17) Brill, A. S.; Fiamingo, F. G.; Hampton, D. A.; Levin, P. D.; Thorkildensen, R. *Phys. Rev. Lett.* **1985**, *54*, 1864−1867.
(18) Yang, A. S.; Gaffney, B. J. *Biophys. J.* **1987**, *51*, 55−67.
(19) Hendrich, M. P.; Debrunner, P. G. *J. Magn. Reson.* **1988**, *78*, 133−141.
(20) Hendrich, M. P.; Debrunner, P. G. *Biophys. J.* **1989**, *56*, 489−506.
(21) Salerno, J. C. *Biochem. Soc. Trans.* **1983**, *13*, 611−615.
(22) Hearshen, D. O.; Hagen, W. R.; Sands, R. H.; Grande, H. J.; Crespi, H. L.; Gunsalus, I. C.; Dunham, W. R. *J. Magn. Reson.* **1986**, *69*, 440−459.
(23) Cannistraro, S. *J. Phys.* (*Paris*) **1990**, *51*, 131−139.
(24) George, G. N.; Bray, R. C. *Biochemistry* **1984**, *22*, 5543−5452.
(25) Carnahan, J. E.; Mortenson, L. E.; Mower, H. F.; Castle, J. E. *Biochim. Biophys. Acta* **1960**, *44*, 520−529.
(26) Mortenson, L. E.; Valentine, R. C.; Carnahan, J. E. *J. Biol. Chem.* **1963**, *238*, 794−800.
(27) (a) Zumft, W. G.; Mortenson, L. E. *Eur. J. Biochem.* **1973**, *35*, 401−409. (b) Mortenson, L. E.; Bare, R.; Morgan, V. P.; Cramer, S. P.; Webb, M. *Nitrogen Fixation Res. Prog., Proc. Int. Symp., 6th.* **1985**, 577−583.
(28) Yang, S.-S.; Pam, W. H.; Friesen, G. D.; Burgess, B. K.; Corbin, J. L.; Stiefel, E. I.; Newton, W. E. *J. Biol. Chem.* **1982**, *257*, 8042−8048.
(29) George, G. N.; Prince, R. C.; Kipke, C. A.; Sunde, R. A.; Enemark, J. E. *Biochem. J.* **1988**, *256*, 307−309.
(30) Abragam, A.; Bleaney, B. *Electron Paramagnetic Resonance of Transition Ions*; Clarendon Press: Oxford, U.K., 1970.
(31) Collison, D.; Mabbs, F. E. *J. Chem. Soc., Dalton Trans.* **1982**, 1565−1982.
(32) Nettar, D.; Villafranca, J. J. *J. Magn. Reson.* **1985**, *64*, 61−65.
(33) Note that there are typographical errors in the expression for transition probability in ref 32.
(34) Wilkinson, J. H.; Reinch, C. *Linear Algebra, Handbook for automatic Computation*; Springer Verlag: New York, 1971; Vol. II.
(35) Smith, B. T.; *et al. Matrix Eigensystem Routines−EISPAK Guide*, 2nd ed.; Lecture Notes in Computer Science, Vol. 6; Springer Verlag: New York, 1976.
(36) van Veen, G. *J. Magn. Reson.* **1978**, *30*, 91−109.
(37) Wasserman, E.; Snyder, L. C.; Yager, W. A. *J. Chem. Phys.* **1964**, *41*, 1763−1772.
(38) Aasa, R.; Vånngård, T. J. *Magn. Reson.* **1975**, *19*, 308−315.

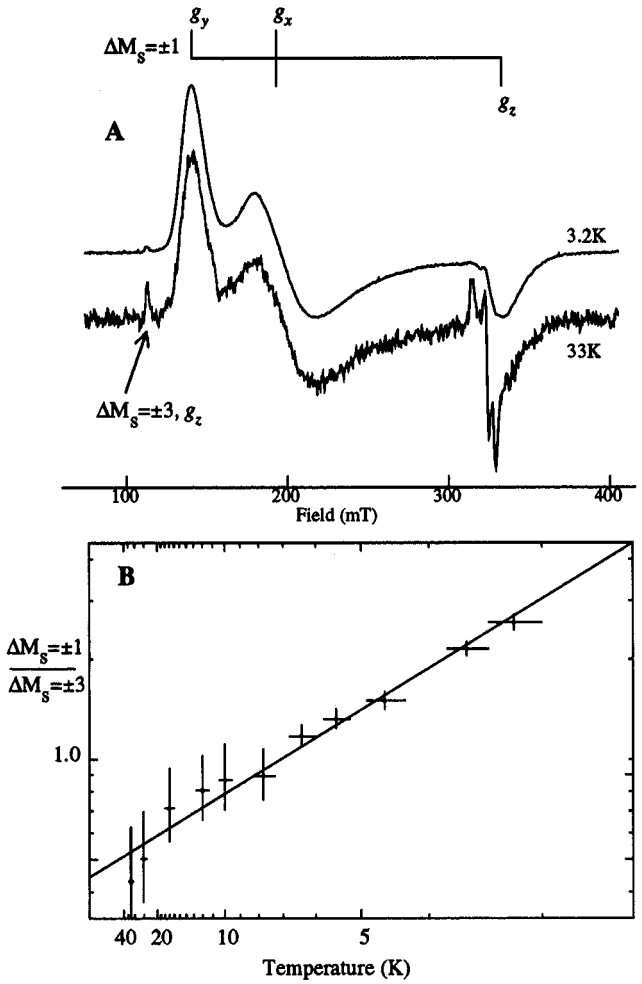

Figure 1. Temperature dependence of the FeMo-co EPR spectrum. (A) EPR spectra at two different temperatures, with the vertical scale adjusted to facilitate comparison. The rhombic EPR signal near $g = 2$ (~330 mT) which is most pronounced in the high-temperature spectrum is commonly attributed to an impurity. (B) Ratio plot of the intensities of the $\Delta M_s = \pm3$ g'_z and $\Delta M_s = \pm1$ g'_y features as a function of sample temperature. A crude estimate of the zero-field splitting parameter D, calculated from the slope of the ratio plot, is 2 cm^{-1}. The abscissa and ordinate of the figure are plotted as reciprocal and logarithmic scales, respectively. The errors shown are approximate only and were estimated by assuming a 5% accuracy in temperature (abscissa) and from the amplitude fo the high-frequency noise (ordinate) in each spectrum.

anisotropy derives almost entirely from the zero-field splitting.[30] In the present work, we adopt the convention of Blumberg,[39] which stipulates that $0 \leq \lambda \leq 1/3$. Correspondingly, the $g' =$ 4.7, 3.2, and 2.0 features correspond to the y, x, and z axes of **D** and are thus labeled g'_y, g'_x, and g'_z. The small feature close to $g' = 6.0$ is the nominally forbidden $\Delta M_s = \pm3$ g'_z transition from within the excited state $\pm3/2$ Kramers doublet. The features arising from $\Delta M_s = \pm3$ g'_x and g'_y are expected at much higher fields and will be extremely broad. The excited state $\pm3/2$ Kramers doublet will thermally depopulate at lower temperatures, and as expected, the intensity of the $\Delta M_s = \pm3$ g'_z feature shows a marked temperature dependence (Figure 1). This can be used to obtain an approximate estimate of the zero-field splitting Δ, and thus of D. Figure 1B shows a plot of the natural logarithm of the ratio of the excited and ground state signal intensities versus the reciprocal of the sample temperature. From the slope of this plot we obtain a value for D of 2 cm^{-1},

(39) Blumberg, W. E. *Wenner-Gren Cent. Int. Symp. Ser.* **1967**, *9*, 119−139.

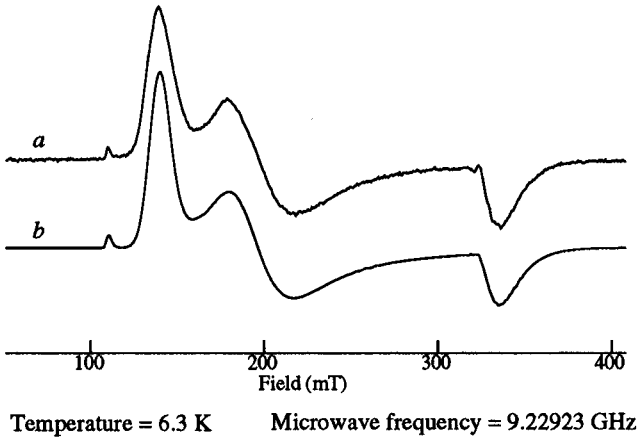

Figure 2. Experimental spectrum (a) and computer simulation (b) of the FeMo-co EPR signal. The computer simulation was calculated using $g_x = 2.030$, $g_y = 2.030$, $g_z = 2.033$, an isotropic line width of 1.0 mT, and zero-field splitting parameters $D = 2.5$ cm^{-1} and $E = 0.32$ cm^{-1}. The distributions in D and E were approximated by Gaussians of half-widths $\sigma_D = 0.45$ cm^{-1} and $\sigma_E = 0.11$ cm^{-1}, respectively. The value of D obtained from the simulation is in good agreement with the value obtained from the temperature dependence measurements shown in Figure 1.

which is much less than the value of 8 cm^{-1} obtained from previous EPR simulations.[31,40] The value is also quite different from that of the M cluster of the intact protein ($D = 5.2$ cm^{-1}) which has been accurately determined from the anisotropic pseudonuclear Zeeman effect in ENDOR spectroscopy.[15] This latter discrepancy emphasizes that there are differences in electronic structure between FeMo-co and the protein-bound cluster.

Computer Simulations. Because of the relative insensitivity of the spectra to the magnitude of D, we at first attempted simulations with Gaussian distributions only in E or λ, with fixed values of D. Yang and Gaffney[18] have successfully used Gaussian distributions only in λ (with fixed values of D) to simulate a number of high-spin Fe^{3+} EPR spectra. Additionally, Hendrich and Debrunner[19,20] have achieved very considerable success in simulating the very broad asymmetric line shapes that are observed for non-Kramers systems, using a distribution only in E. Although capable of reproducing many of the major features of the spectrum, this approach proved unsatisfactory in simulating the FeMo-co EPR signal. The width of the distribution required to reproduce the main spectral features meant that a significant fraction of the values for λ are close to zero. This results in a small but pronounced peak at the axial position ($g' = 4.06$), which is not observed experimentally. The use of Gaussian distributions in both D and E produces a very good simulation of the experimental spectrum, which is shown in Figure 2. In this case, the probability of values for λ close to zero is vanishingly small, and no axial contributions are observed. The asymmetric line shapes in the g'_z and the g'_x region are quite accurately reproduced by the simulation in Figure 2, as are the intensity and peak shape of the $\Delta M_s = \pm3$ g'_z feature. The line shape in the $\Delta M_s = \pm1$ g'_y region is slightly sharper in the simulation than in the data. This may indicate that the assumption of a Gaussian distribution in zero-field

(40) It is also possible that the discrepancy between our estimate of D and previous estimates is due in part to inaccurate temperature control in the earlier work. We consider this possibility unlikely from the similarity between our experimental spectra and those of earlier workers.[13] Furthermore, such discrepancies are expected due to inadequate reproduction of the intensity of particular features when D-strain is excluded from the simulation. Similar discrepancies in values of total integration have been shown to exist between simulations with and without the inclusion of g-strain (*e.g.* ref 22).

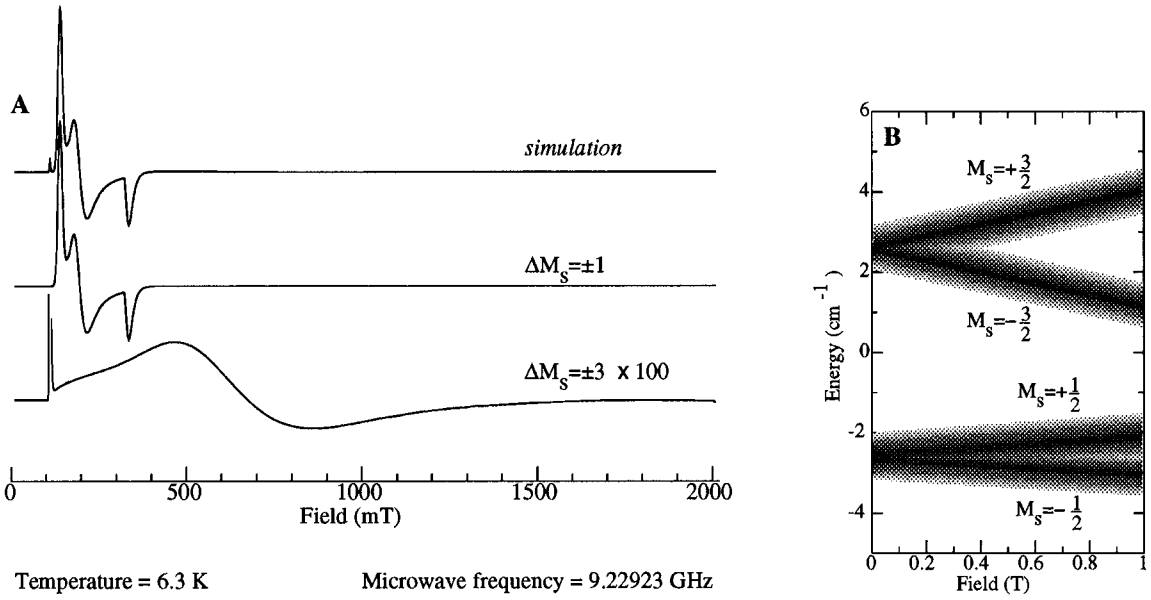

Figure 3. (A) Computer simulation of the FeMo-co EPR signal calculated over a wide field range, together with the $\Delta M_s = \pm 1$ and $\Delta M_s = \pm 3$ components. The vertical scale of the $\Delta M_s = \pm 3$ simulation has been expanded to show the broad high-field structure, and the sharp $\Delta M_s = \pm 3$ g'_z feature near 110 mT has been truncated. (B) Energy-level diagram for FeMo-co, calculated by matrix diagonalization with $S = {}^3/_2$, $D = 2.5$ cm^{-1}, and $E = 0.32$ cm^{-1} and with the magnetic field oriented along z (*i.e.* g'_z). The distribution of energy levels caused by the presence of *D*-strain is indicated semiempirically in the figure by the width of the energy levels.

splitting parameters is an oversimplification. Nevertheless, the striking similarity of the simulated and calculated spectra is excellent evidence for the presence of a distribution in zero-field splittings. In particular, the narrow relative line shape of the $\Delta M_s = \pm 3$ g'_z feature is quite impossible to reproduce with simulations not including *D*-strain. Collision and Mabbs[31] have attempted to simulate the FeMo-co EPR spectrum by modeling the line width anisotropy as though it were unresolved hyperfine coupling, with different sets of linewidths for the $\Delta M_s = \pm 1$ and $\Delta M_s = \pm 3$ transitions, and no *D*-strain. Their estimate for the zero-field splitting parameter D of 8 cm^{-1} is clearly much too large, illustrating the importance of including *D*-strain if one desires to obtain accurate spin-Hamiltonian parameters.

Figure 3 shows the simulated FeMo-co spectra over a wide field range (0.0−2.0 T). Broad features, centered at about $g' \approx 1.0$, are predicted for the $\Delta M_s = \pm 3$ component, effectively arising from g'_y and g'_x. EPR spectra of very broad features such as those predicted in Figure 3 are almost impossible to observe experimentally with conventional field-modulated apparatus, as they are of the same order as the subtle drifts in baseline which always occur, even on the most stable spectrometers. For this reason, and despite considerable effort, we were unable to experimentally confirm the presence of these resonances.

Figure 4 shows the experimental and simulated spectra of the intact nitrogenase protein from *Clostridium pasteurianum*. For the protein spectrum, unlike the case of FeMo-co, we observe very little asymmetry in the individual peaks (see the inset in Figure 4), making the effects of *D*-strain rather more subtle. The overall line shape is adequately reproduced by the simulation, including the very sharp $\Delta M_s = \pm 3$ g'_z region. We note that, as seen for isolated FeMo-co, the width of the simulated $\Delta M_s = \pm 1$ g'_y region is slightly sharper than that of the experimental spectrum. The protein simulation was much less sensitive to the exact values of σ_D and σ_E than was the FeMo-co simulation, and the values of these parameters derived for the protein (Figure 4) should therefore be considered as approximate. In previous work, the relatively small line width of the $\Delta M_s = \pm 3$ g'_z feature has been exploited to directly observe hyperfine couplings in protein samples isotopically

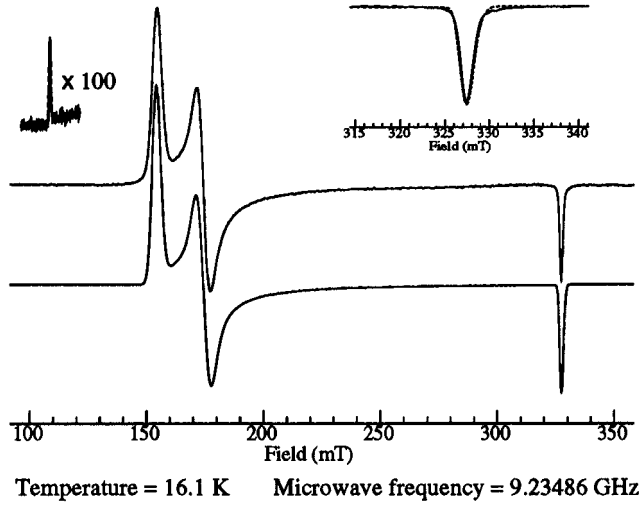

Figure 4. Experimental spectrum (a) and computer simulation (b) of the *C. pasteurianum* M-protein EPR signal. The computer simulation was calculated using $g_x = 2.016$, $g_y = 2.016$, $g_z = 2.024$, an isotropic line width of 0.5 mT, and zero-field splittings $D = 5.2$ cm^{-1} and $E = 0.21$ cm^{-1}. The distributions in D and E were approximated by Gaussians of half-widths $\sigma_D = 0.073$ cm^{-1} and $\sigma_E = 0.044$ cm^{-1}, respectively. The value of D was fixed at a literature value.[15]

enriched with the stable magnetic isotopes ^{57}Fe and ^{95}Mo (in the form of resolved structure and line shape broadening, respectively).[14] This work unambiguously showed that the ^{95}Mo hyperfine coupling A_z is in fact 2.9 MHz rather than 8.1 MHz determined from analysis of ENDOR spectra.[15,16]

For a system involving only a single magnetically isolated paramagnetic metal ion, the magnitude of the zero-field splitting can be shown to be simply related to the ligand field environment of the metal.[41] *D*-strain in such a system may be related to variations in the ligand fields, which are expected in the presence of local stresses such as might be present in frozen solutions[42] or in the presence of structural flexibility. The use

(41) Newman, D. J.; Urban, W. *Adv. Phys.* **1975**, *24*, 793−844.
(42) Kliava, J. *J. Phys. C.* **1982**, *15*, 7017−7029.

of a simple ligand field approach, the so-called superposition model,[41] has even been used to quantitatively analyze zero-field splittings for isolated metal ions (*e.g.* refs 41−43). In FeMo-co, the unpaired electrons are delocalized over a structurally complex cluster[5,6,8,14−16] with significant spin density on sulfur, iron, and molybdenum atoms,[14−16] and the origins of the zero-field splittings are clearly much more complicated. Thus it is not, at present, possible to apply quantitative theory to the zero-field splittings of the iron-molybdenum cofactor.

In the case of FeMo-co, *D*-strain almost certainly has its origins in slight geometrical variations in the cluster, such as the capability of cluster components or side chains to move, in which case the degree of *D*-strain will be a function of the width of the distribution of the ensemble of conformational substrates.[44] Thus, *D*-strain might be expected to be rather more pronounced in solutions of the isolated cofactor than in the intact protein, as the conformational flexibility of the cluster might be rather more rigidly constrained in the latter. We wish to emphasize the fact that the presence of broad, asymmetric EPR line shapes due to *D*-strain is an intrinsic molecular property of the system and does not indicate a lack of chemical homogeneity, as has been commonly supposed by others (*e.g.* ref 45). In the case of FeMo-co, the *D*-strain appears to be quantitatively reproducible, being quite insensitive to cofactor concentration (data not shown) and to sample temperature and invariant from preparation to preparation; there is no evidence from EPR spectroscopy to suggest that FeMo-co solutions are chemically inhomogeneous. The large *D*-strain effect in FeMo-co might have significance for understanding the catalytic mechanism of the protein, perhaps indicating the presence of inherent structural flexibility of the iron−molybdenum cluster (once released from a restraining protein backbone) such as might be required to bind N_2 during the catalytic cycle.[12]

Acknowledgment. This work was done partially at SSRL, which is funded by the Department of Energy, Office of Basic Energy Sciences. The Biotechnology Program is supported by the NIH, Biomedical Research Technology Program, Division of Research Resources. Further support was provided by the Department of Energy, Office of Health and Environmental Research.

IC950740M

(43) Büscher, R.; Lehmann, G. *Z. Naturforsch.* **1987**, *42A*, 67−71.
(44) Bizzarri, A. R.; Bacci, M.; Cannistraro, S. *Biophys. Chem.* **1993**, *46*, 117−129.
(45) Ma, L.; Gavini, N.; Liu, H. I.; Hedman, B.; Hodgson, K. O.; Burgess, B. K. *J. Biol. Chem.* **1994**, *269*, 18007−18015.